Bioorganic & Medicinal Chemistry Letters xxx (2014) xxx–xxx

Contents lists available at ScienceDirect

Bioorganic & Medicinal Chemistry Letters

journal homepage: www.elsevier.com/locate/bmcl

Structure-based optimization of non-peptidic Cathepsin D inhibitors

Ulrich Grädler [a,*], Paul Czodrowski [a], Christos Tsaklakidis [a], Markus Klein [a], Daniela Werkmann [a], Sven Lindemann [a], Klaus Maskos [b], Birgitta Leuthner [a]

[a] Merck KGaA, Merck Serono Research, Small Molecule Platform, Frankfurter Str. 250, 64293 Darmstadt, Germany
[b] Proteros Biostructures GmbH, Bunsenstrasse 7a, 82152 Martinsried, Germany

ARTICLE INFO

Article history:
Received 30 April 2014
Revised 15 July 2014
Accepted 18 July 2014
Available online xxxx

Keywords:
Cathepsin D
Non-peptidic inhibitor
X-ray structure
Structure-based design

ABSTRACT

We discovered a novel series of non-peptidic acylguanidine inhibitors of Cathepsin D as target for osteoarthritis. The initial HTS-hits were optimized by structure-based design using CatD X-ray structures resulting in single digit nanomolar potency in the biochemical CatD assay. However, the most potent analogues showed only micromolar activities in an ex vivo glycosaminoglycan (GAG) release assay in bovine cartilage together with low cellular permeability and suboptimal microsomal stability. This new scaffold can serve as a starting point for further optimization towards in vivo efficacy.

Cathepsin D (CatD, EC 3.4.23.5) belongs to the large family of aspartic proteases involved in peptide bond hydrolysis via an acid–base mechanism mediated by two catalytic aspartates.[1–3] CatD is found in lysosomes of most mammalian tissues and initially synthesized as preprocathepsin in the rough endoplasmic reticulum.[4,5] Further processing by removal of an N-terminal signal peptide results in the 52 kDa procathepsin D (pCD) representing an inactive zymogene at neutral pH due to propeptide segments blocking the active site. The proenzyme is auto activated under acidic conditions in the lysosome by removal of the 44 amino acid N-terminal propeptide leading to a 48 kDa single chain intermediate active enzyme form. Final proteolytic cleavage results in a mixture of single and two-chain molecules composed of heavy (34 kDa) and light (14 kDa) chains linked by non-covalent interactions in a globular structure.[6–9]

Cathepsin D is a target for cancer, inflammation, and osteoarthritis. In osteoarthritis (OA), CatD seems to be directly involved in pathophysiological events resulting in degeneration of the hyaline cartilage. Cathepsin D is expressed on mRNA and protein level in the chondrocytes and its catalytic activity correlates directly with the severity of OA.[10] Cathepsin D cleaves aggrecan at unique sites resulting in a beginning degradation of the extracellular matrix, which is necessary for the unique biomechanical properties of hyaline cartilage of diarthrodial joints.[11] Several CatD inhibitors are published bearing peptidic scaffolds such as pepstatin A (**1**, Fig. 1) which contains the unusual amino acid (3*S*,4*S*)-4-amino-3-hydroxy-6-methylheptanoic acid (statine) mimicking the tetrahedral transition state of peptide catalysis. Pepstatin A (**1**) was discovered in various strains of actinomyces and inhibits several aspartic proteases including pepsin (IC_{50} ~0.1 nM), Cathepsins D (IC_{50} < 1 nM) and E (IC_{50} < 7.5 nM).[12,13] The therapeutical potential of pepstatin A (**1**) is hindered by its low intracellular penetration, but recently reported conjugates demonstrated antiproliferative effects on tumour cell cultures.[14] Highly potent CatD inhibitors containing a hydroxyethylamine aspartyl protease isostere as in **2** (K_i = 0.7 nM, IC_{50} = 85 nM) were identified by solid-phase synthesis of a small combinatorial library.[15] Non-peptidic CatD inhibitors with alternative chemical scaffolds such as the benzophenone rhodanine **3** (IC_{50} = 210 nM) or the diarylsulfonamide **4** (IC_{50} = 250 nM) were published by Eli Lilly and Bayer, respectively.[16,17]

In a high-throughput screening campaign conducted on our corporate compound library, we identified a series of acylguanidine **5**–**14** as potent inhibitors of human CatD with IC_{50}s in the range between 440 nM and 29 μM (Table 1).[18] This chemo type served as interesting starting point because of its non-peptidic scaffold with preferred lead-like properties and ligand binding efficiencies (LE ~0.3). In addition, the HTS-hits were inactive below 30 μM against the structural closely related aspartic protease renin.[19] Renin controls the first step of the renin–angiotensin–aldosterone system (RAAS) regulating the blood pressure and was considered as an off-target.[20] The acylguanidine moiety has been reported as specific binder forming key H-bond interactions

* Corresponding author. Tel.: +49 6151 725975; fax: +49 6151 72915975.
E-mail address: ulrich.graedler@merckgroup.com (U. Grädler).

http://dx.doi.org/10.1016/j.bmcl.2014.07.054
0960-894X/© 2014 Elsevier Ltd. All rights reserved.

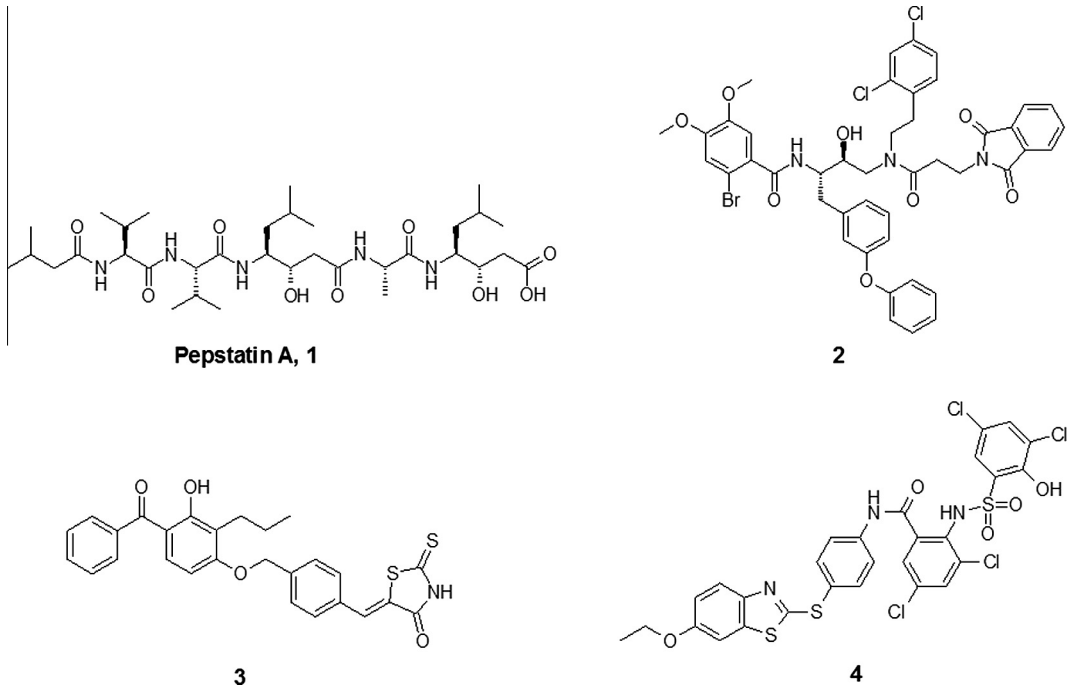

Figure 1. Published Cathepsin D inhibitors.

to the two catalytic aspartic acids of the structurally related aspartic protease BACE-1.[21]

For further structure-based optimization, we co-crystallized a recombinant human form of CatD (rhCatD) with the acylguanidine **7** and solved the structure at 2.9 Å resolution (Supplementary Table 1).[22,23] An X-ray structure analysis revealed three specific H-bonds between the mono substituted and presumably protonated amino group of the acylguanidine **7** and the side chains of the catalytic Asp33 and Asp231 in the active site cleft of CatD (Fig. 2a). The N^1-acylated amino group of **7** forms an additional H-bond to Asp231, while the N^2-guanidine atom is involved in an intramolecular H-bond interaction with the carbonyl O-atom of the acyl group. Consequently, the acylguanidine moiety adopts a pseudo 6-membered ring with a $z(N^1)$ and $e(N^2)$ configuration. This spatial arrangement positions the 4-methylbenzyl group of **7** into the S_3'-subpocket of CatD with lipophilic interactions to Ile311, Ile320 and Tyr205. The binding interactions correspond with the initial SAR indicating a preference for lipophilic substituents in the 4-position of the benzyl group such as the most active 3,4-chloro derivative **5** (IC_{50} = 440 nM). In contrast, a significant drop in binding affinity is observed for the 4-amino derivative **14** (IC_{50} = 29 μM). The 3,4-dimethoxyphenyl substituent is bound into the S_1- and S_3-subpockets with lipophilic contacts to Thr125, Phe131 and Ile134 (Fig. 2a). The benzyl linker of **7** is involved in van-der-Waals interactions to Tyr78 and derivatives with an ethyl or *n*-propyl linker like **12** (IC_{50} = 18 μM) and **13** (IC_{50} = 25 μM) were lower active (Table 1).

The biochemically most active compounds from the HTS-series were also tested in an ex vivo assay measuring the glycosaminoglycan (GAG) release in bovine cartilage explants. Briefly, bovine cartilage explants were prepared from the metacarpal phalangeal joint of 1–2 year old cows at the day of slaughter, provided from a local slaughter house. The GAG content of the explants was determined with a spectrophotometric 1,9-dimethylmethylene blue shift assay and revealed high potency for pepstatin A (**1**, IC_{50} = 1.5 nM).[24,25] However, the acylguanidines **5**–**9** as well as the hydroxyethylamine reference inhibitor **2** did not show inhibition of GAG-release below 1 μM. Our next goal was therefore the improvement of binding affinity by targeting additional subpockets of the large CatD binding cleft. The X-ray structure of human CatD in complex with pepstatin A (**1**) revealed the specific occupation of six subpockets by the various amino acid side chains of the inhibitor each contributing to the observed subnanomolar binding affinity (Fig. 2b).[26] We determined the crystal structure of rhCatD in complex with the reference inhibitor **2** at 2.6 Å resolution (Supplementary Table 1) for additional guidance of our structure-based design campaign. The inhibitor **2** forms several H-bonds within the CatD binding cleft between the following residues: (1) statine OH-group and the catalytic Asp231/Asp33, (2) both amide carbonyl O-atoms and Gly79/Ser80 of the flap region and (3) both methoxy O-atoms and Ser235 (Fig. 3a). The lipophilic substituents of the hydroxyethylamine derivative **2** are placed into six subpockets: the 3-phenoxy-benzyl ring in S_1 and S_3, the 2-bromo-4, 5-dimethoxy benzamide group in S_2 and S_4, the phthalimide ring in S_2' and the 2,5-dichlorophenyl moiety in S_3' (Fig. 3a). The structural superimposition of CatD·**2** and CatD·**7** indicates four available subpockets (S_2, S_3, S_4 and S_2') for the introduction of additional substituents to the acylguanidine scaffold (Fig. 3b). The benzyl position of the P_3'-residues adjacent to the N^2-guanidine atom ('branching position') offers suitable vectors to address the S_2 or S_2' subpocket, which was further underlined by SZMAP calculations (Fig. 4). This method predicts the occurrence of water sites based on implicit solvent Poisson Boltzmann calculations.[27] SZMAP revealed water sites with a hydrophilic character in the vicinity of the 'branching position' and Ser80 of the flap region, suggesting the introduction of an amide substituent as linker to target the S_2 or S_3' subpocket. At the elongation of the amide linker, a pocket formed by Thr234, Met309 and Ile320 is found which accommodates water sites with a hydrophobic character.

We prepared a library of follow-up acylguanidines according to Scheme 1 (see Supplement).[28] Additional substituents in the 'branching position' such as phthalimide or 3,4-dimethoxybenzyl were inspired by superimposition with the reference compound **2** and prior evaluated by docking (data not shown). Initial derivatives bearing benzyl- and N-phthalimide ethyl amide substituents in the 'branching position' were tested as separated enantiomers

Table 1
Structure–activity relationship of acylguanidine HTS-series against human Cathepsin D and renin

Compound	Structure	Cathepsin D		Renin
		IC_{50}[a] (μM)	LE[b]	IC_{50}[c] (μM)
5	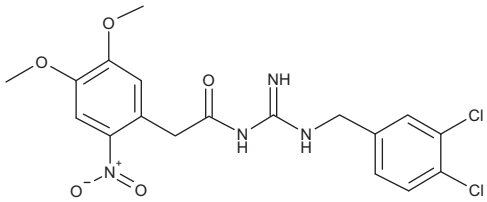	0.44	0.3	>30
6	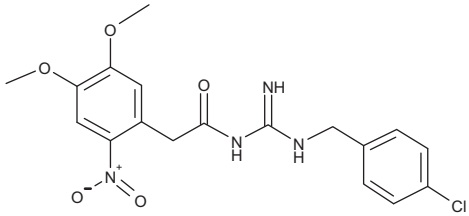	1.5	0.28	>30
7	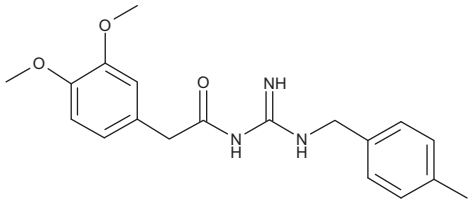	1.9	0.31	>30
8	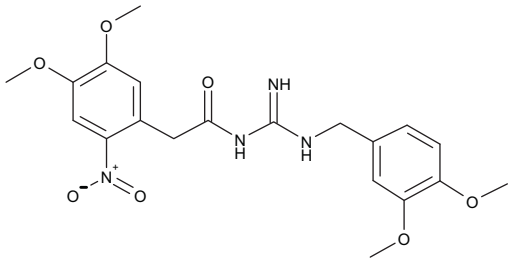	2.7	0.25	>30
9	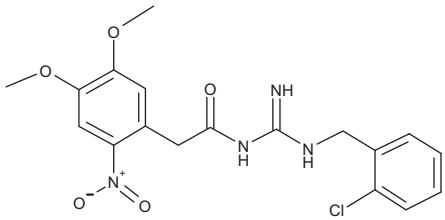	3.0	0.27	>30
10	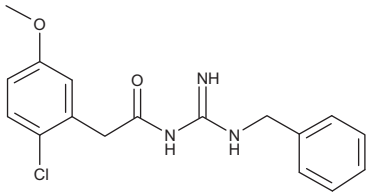	6.1	0.31	>30
11	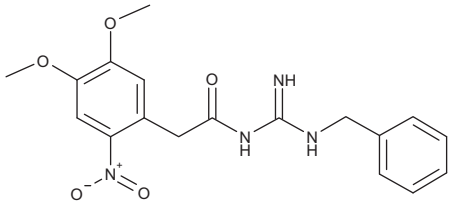	10	0.26	>30

(*continued on next page*)

Table 1 (*continued*)

Compound	Structure	Cathepsin D		Renin
		IC_{50}[a] (μM)	LE[b]	IC_{50}[c] (μM)
12	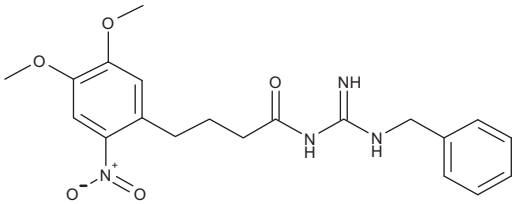	18	0.22	>30
13	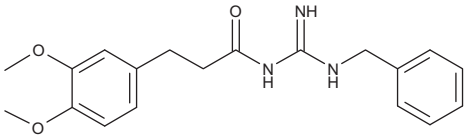	25	0.25	20
14	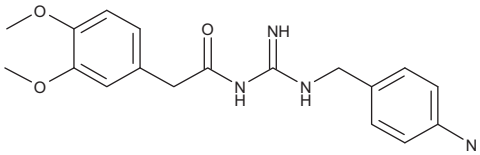	29	0.25	>30

[a] Cathepsin D biochemical assay.[18]
[b] Ligand binding efficiencies (LE) based on the biochemical IC_{50}.
[c] Renin biochemical assay.[19]

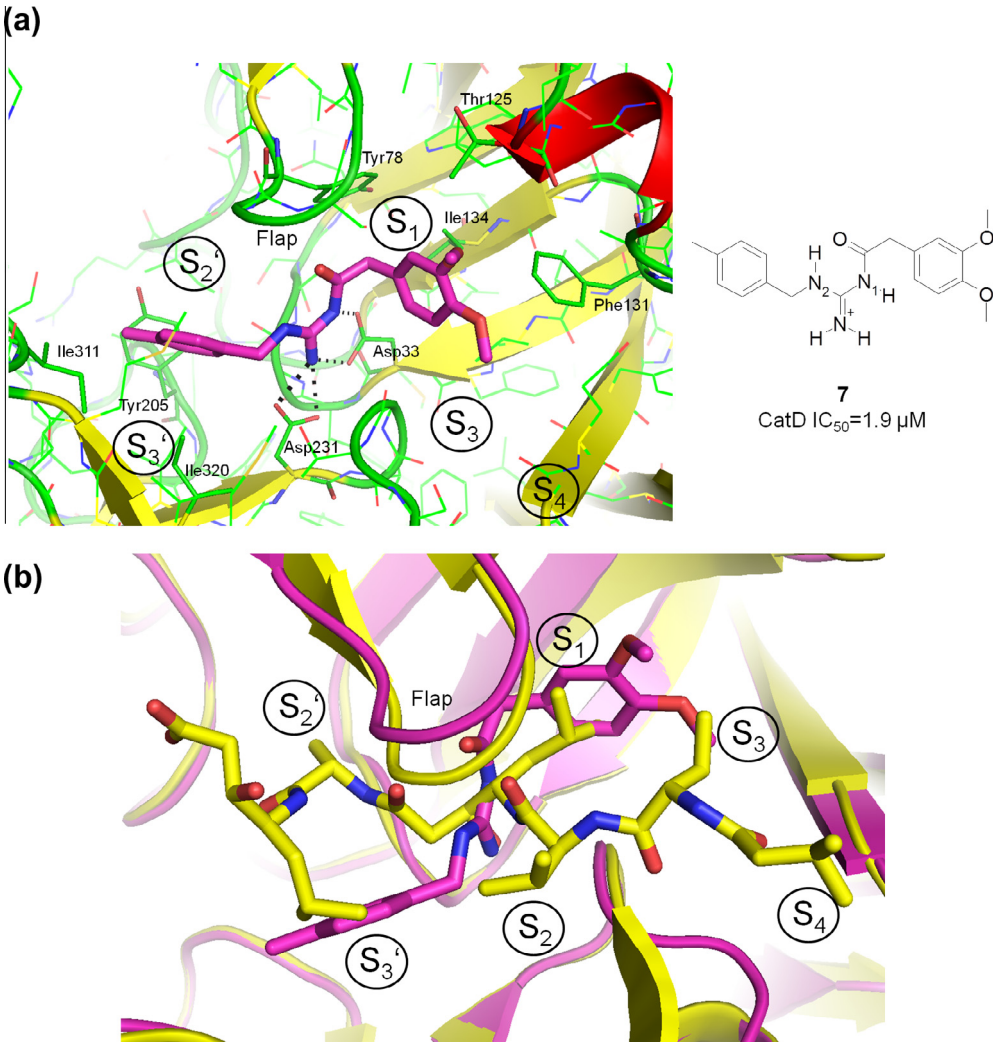

Figure 2. (a) X-ray structure of human CatD in complex with **7** (magenta, PDB-ID: 4obz). H-bonds to the catalytic Asp231 and Asp33 are represented as dashed lines. (b) Superimposition of CatD X-ray structures in complex with **7** (magenta, PDB-ID: 4obz) and pepstatin A (yellow, PDB-ID: 1lyb, **1**) and subpocket positions.

Please cite this article in press as: Grädler, U.; et al. *Bioorg. Med. Chem. Lett.* (2014), http://dx.doi.org/10.1016/j.bmcl.2014.07.054

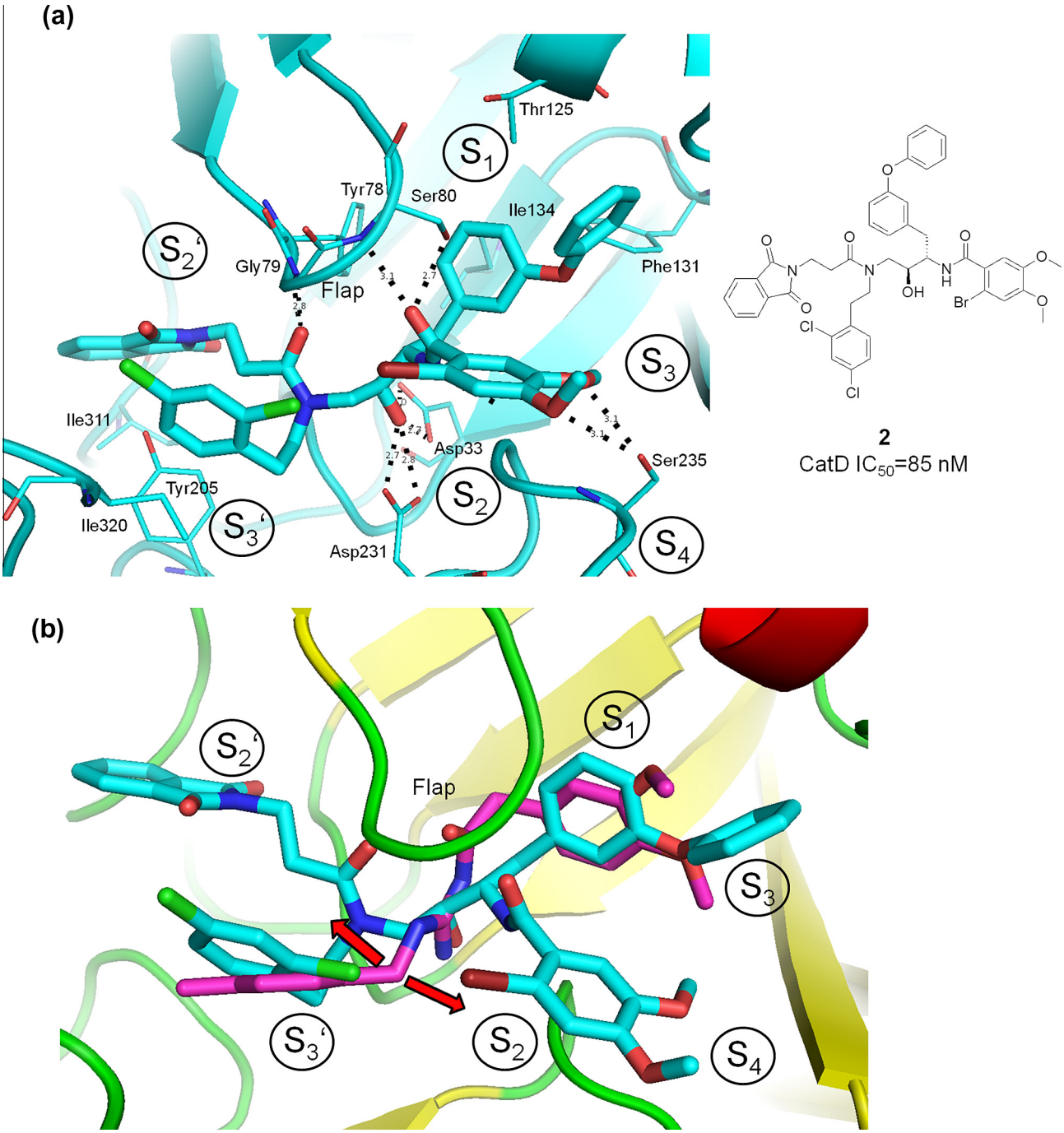

Figure 3. (a) X-ray structure of CatD in complex with the reference inhibitor **2** (blue, PDB-ID: 4oc6, H-bonds represented as dashed lines). (b) Superimposition of CatD X-ray structures with the HTS-hit **2** (magenta, PDB-ID: 4oc6) and the reference inhibitor **7** (cyan, PDB-ID: 4obz). The red arrows mark the substitution position at the benzyl substituent of **2** for targeting the S_2 or S_2' subpockets to improve binding affinity.

with assigned stereochemistry (Table 2). Interestingly, both enantiomers revealed significant potency differences in the CatD assay (**22**: IC_{50} = 320 nM; **23**: IC_{50} = 8.3 μM) as well as against renin (**22**: IC_{50} = 27 μM; **23**: IC_{50} = 8.4 μM). For further clarification, we co-crystallized the analogue **24** with an improved CatD potency (IC_{50} = 58 nM) and inactivity against renin below 30 μM in CatD. The X-ray structure of rhCatD·**24** revealed an R-configuration in the 'branching position' with the benzyl ring bound into the S_3' subpocket (Fig. 5a). To our surprise, the S_2' subpocket was unoccupied and the 3,4-methoxybenzyl amide substituent was oriented towards the interface of the S_2 and S_3' subpockets (Fig. 5b). In this binding mode, the amide group at the 'branching position' forms additional H-bonds with Gly79 of the flap region and Thr234 in the S_3' subpocket (Fig. 5a). The 3,4-methoxybenzyl substituent induces a side chain rotation of Met309 to accommodate the aromatic ring sandwiched between Met309 and the backbone amide of Gly79 of the flap hairpin loop. Protein–inhibitor interactions calculated with the software tool ViewContacts revealed van-der-Waals contacts between the 3,4-methoxybenzyl substituent and Met309 in addition to H-donor–π contacts to Gly79 (Fig. 5a).[29] This new crystal structure in combination with SZMAP calculations served as template for further optimization of the acylguanidines.

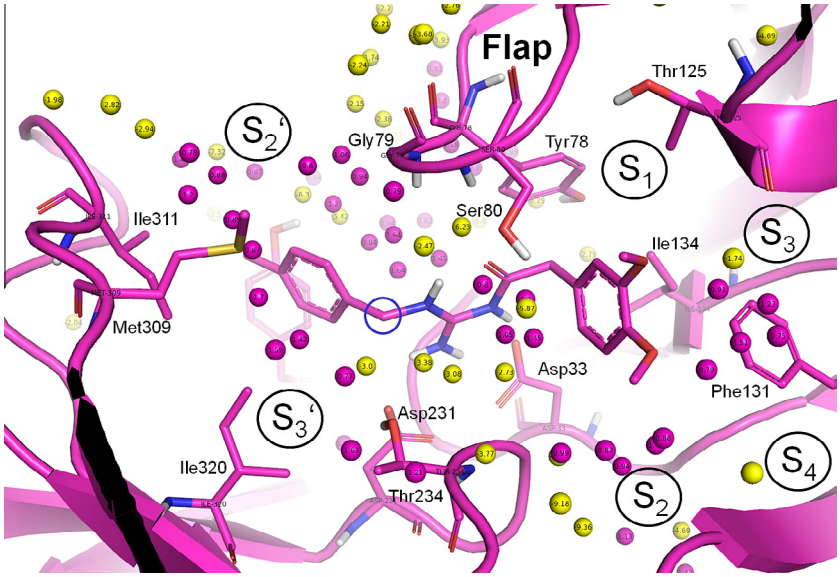

Figure 4. SZMAP calculation for the HTS hit **7**. Yellow sites correspond to hydrophilic sites, whereas pink sites correspond to hydrophobic sites. Our design strategy was to introduce suitable substituents into the branching position (blue circle) to fill the S_3'/S_2 pockets.

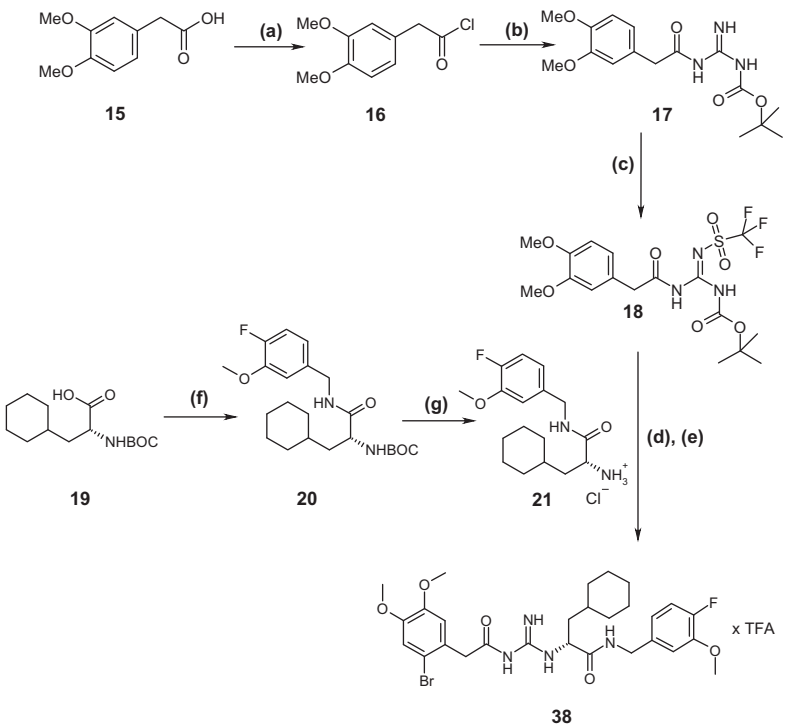

Scheme 1. Reagents and conditions: (a) $(COCl)_2$, DCM, rt, 96%; (b) N-BOC-guanidine, 82%; DCM, DIPEA, −10 °C; (c) $(CF_3SO_2)_2O$, TEA, −70 °C, N21) , 59%; (d) THF, DIPEA, rt; (e) TFA, DCM, rt, 49% for steps (d and e); (f) 4-Fluoro-3-methoxy-benzylamine xHCl, *N*-methyl-morpholine, EDCI, HOBt, DMF, rt, 100%; (g) 4 N HCl in dioxane, rt, 100%.

The improved biochemical CatD potency of **24** was already sufficient to reach submicromolar inhibition in the GAG-assay (IC_{50} = 330 nM), but we also observed high in vitro clearance (Cl_{int}) values in human and rat liver microsomes (>1000 and 384 μL/min/mg) for this derivative (Table 3).[30–32] A sufficient stability in human liver microsomes (Cl_{int} < 10 μL/min/mg) was one major parameter in our hit-optimization strategy towards a lead candidate for targeting human CatD against OA. Therefore, our next attempt was to replace metabolically labile groups in the molecule, which are e.g. prone to demethylation or benzyl oxidation to improve the in vitro clearance. Substitution of the benzyl group in **24** by cyclohexyl or isobutyl to more optimally fill the S_3' subpocket retained CatD-potency (**25**: IC_{50} = 120 nM; **26**: IC_{50} = 67 nM) and slightly improved human and rat Cl_{int}-values for **26** (262 and 143 μL/min/mg). Further reduction of the polar surface area (PSA) by subsequent replacement of one or both methoxy groups of the S_2/S_3' benzyl amide substituent by fluorine as in **27**–**30** resulted in enhanced CatD-potency (**30**: IC_{50} = 24 nM). This SAR well corresponds with the observed contacts of **24** in the S_2/S_3' pocket suggesting improved van-der-Waals and/or H-donor–π

Table 2
SAR of optimized acylguanidines against human Cathepsin D and renin

Compound	Structure	Cath D IC_{50}[a] (μM)	GAG (bovine) IC_{50}[b] (μM)	Renin IC_{50}[c] (μM)
22	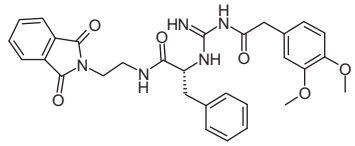	0.32	ND	27
23	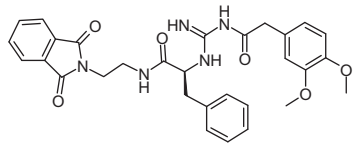	8.3	ND	8.4
24	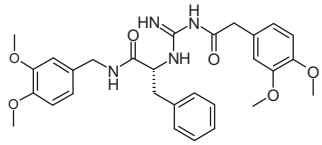	0.058	0.33	>30
25	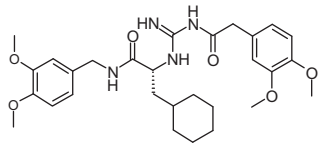	0.12	ND	ND
26	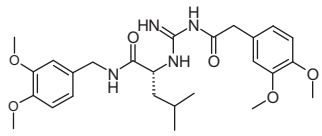	0.067	ND	ND
27	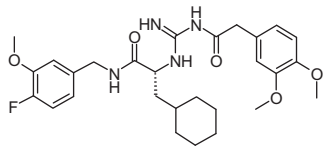	0.170	0.5	16
28	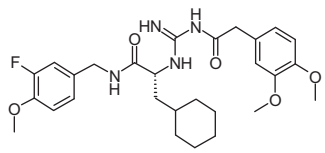	0.098	ND	13
29	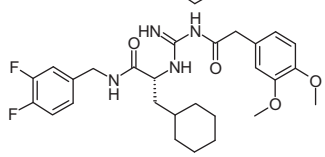	0.170	ND	ND
30	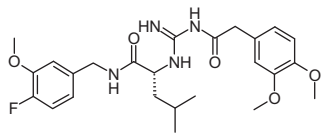	0.024	0.62	8.7
31	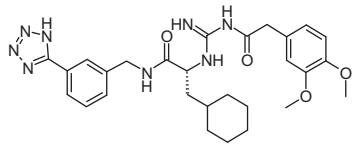	0.092	ND	ND
32	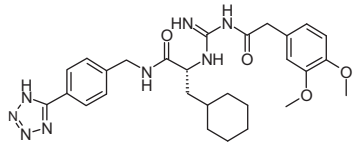	0.044	1.8	ND

(*continued on next page*)

Table 2 (*continued*)

Compound	Structure	Cath D IC_{50}[a] (μM)	GAG (bovine) IC_{50}[b] (μM)	Renin IC_{50}[c] (μM)
33	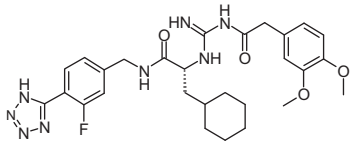	0.081	ND	ND
34	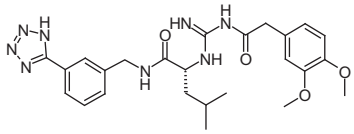	0.370	ND	ND
35	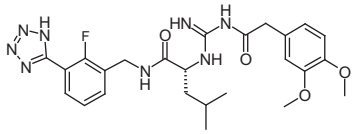	0.280	ND	ND
36	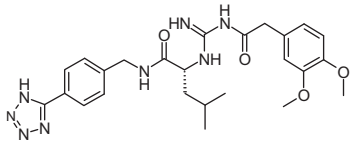	0.510	ND	ND
37	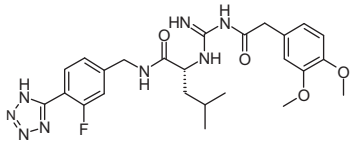	0.690	ND	ND
38	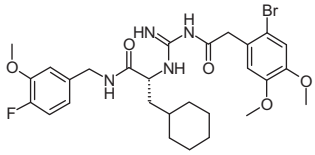	0.0086	0.9	>30
39	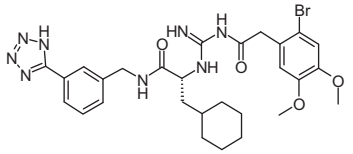	0.140	ND	ND
40	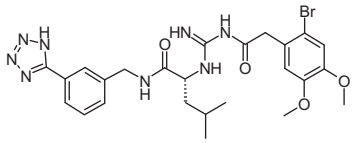	0.240	ND	ND

[a] Cathepsin D biochemical assay.[18]
[b] Glycosaminoglycan (GAG) release in bovine cartilage explants (ex vivo).[25] ND = not determined.
[c] Renin biochemical assay.[19] ND = not determined.

interactions to Met309 by fluorine atoms replacing the methoxy groups. However, the enhanced biochemical CatD affinity of the best fluorine derivatives did not result in potency gains in the GAG-assay (**27**: IC_{50} = 0.5 μM; **30**: IC_{50} = 0.62 μM). Furthermore, the microsomal stabilities of **27** and **30** were not further improved in comparison to **24** and we still detected significant renin activity (**30**: IC_{50} = 8.3 μM). A major step forward in Cl_{int} optimization was the introduction of a tetrazole in the *meta*- or *para*-position of the benzyl amide substituent targeting the S_2/S_3' subpocket as exemplified by **31**–**37**. We obtained tetrazoles such as **36** with already low mouse and rat Cl_{int}-values (<10 μL/min/mg) and **37** with a medium clearance (54 μL/min/mg) in human liver microsomes (Table 3). All tetrazole derivatives revealed submicromolar CatD activity in agreement with the rhCatD·**24** X-ray structure indicating available space for the tetrazole ring in the interface between Met309 and Gly79 (Table 2). Interestingly, a reversed SAR was observed for the *meta*- or *para*-substituted tetrazoles with a cyclohexyl (*meta* **31**: IC_{50} = 92 nM; *para* **32**: IC_{50} = 44 nM) or isobutyl group (*meta* **34**: IC_{50} = 370 nM; *para* **36**: IC_{50} = 510 nM) bound to the adjacent S_3' subpocket. But still the most potent tetrazole derivative **32** (CatD IC_{50} = 44 nM) showed only weak inhibition in the GAG-assay (IC_{50} = 1.8 μM).

Finally, we focussed our optimization efforts on the S_1/S_3 subpockets and achieved single digit nanomolar CatD inhibition (**38**: IC_{50} = 8.6 nM) by the introduction of a 2-bromo-4,5-dimethoxyphenyl substituent as present in the reference inhibitor **2**. However, **38** revealed only moderate activity in the GAG-assay (IC_{50} = 0.9 μM) and high human and rat Cl_{int}-values (>1000 and 823 μL/min/mg). The introduction of a tetrazole in the S_2/S_3' subpocket as in **39** and **40** again improved the microsomal clearance

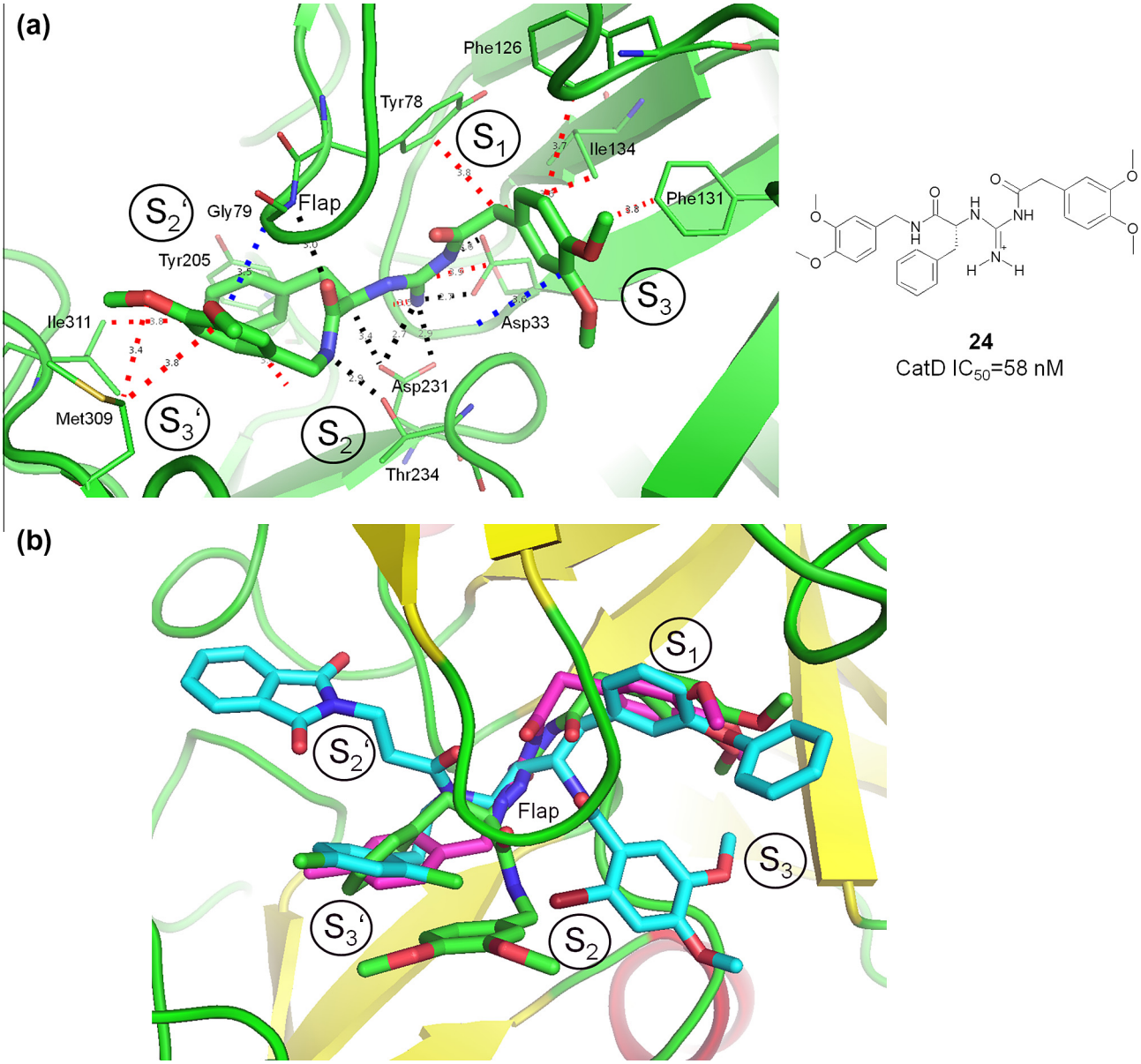

Figure 5. (a) X-ray structure of human CatD in complex with an optimized acylguanidine **24** (green, PDB-ID: 4od9). Favourable interactions between protein and inhibitor atoms were calculated with the software tool ViewContacts and represented as dashed, coloured lines (black: H-bonds, red: van-der-Waals contacts, blue: H-donor–π interactions). (b) Superimposition of CatD X-ray structures with the HTS-hit **2** (magenta, PDB-ID: 4oc6), the reference inhibitor **7** (cyan, PDB-ID: 4obz) and the optimized acylguanidine **24** (green, PDB-ID: 4od9).

Table 3
Physicochemical properties and in vitro ADME parameters for selected compounds

Compound	Microsomal stability Cl_{Int}[a] (μL/min/mg)			Caco-2 cell permeability		tPSA[b] (Å^2)
	Human	Rat	Mouse	P_{app} a→b (cm/s)	Efflux ratio	
24	>1000	384	ND	ND	ND	131
26	262	143	ND	ND	ND	131
27	>1000	241	ND	5·10e-6	26	122
30	966	148	ND	ND	ND	122
32	76	38	<10	0.25·10e-6	34	167
36	69	<10	<10	ND	ND	167
37	54	<10	ND	ND	ND	167
38	>1000	823	ND	ND	ND	122
39	240	33	40	ND	ND	167
40	107	17	38	ND	ND	167

[a] The in vitro clearance was measured in human, mouse and rat liver microsomes (ND = not determined).
[b] The topological surface area (tPSA) was calculated with MOE.[41]

(10–50 μL/min/mg in mouse and rat), but also resulted in a ~20-fold drop in CatD potency. The final show stopper for further in vivo profiling of the most active derivatives in the GAG-assay was the low permeability. The compounds **27** (P_{app} a→b = 5 10e-6 cm/s; efflux ratio = 26) and especially **32** (P_{app} a→b = 0.25 10e-6 cm/s; efflux ratio = 34) were unable to show sufficient cell penetration, which might explain the observed drops between enzymatic and cellular potencies (**27**: 3-fold; **32**: 40-fold, Tables 2 and 3).

In summary, our optimization strategy resulted in acylguanidines with low nanomolar CatD potency together with an aspired selectivity profile against renin. However, the most potent analogues showed only micromolar activities in the explant assay together with low microsomal stability and permeability. The polar surface area of the most potent derivatives need to be further reduced (<120) to improve cellular potency and intestinal permeability.[33] This might be achieved by diminishing the number of nitrogen and oxygen atoms in the overall molecule including the acylguanidine group, which forms a pseudo 6-membered ring in the bioactive conformation. A meaningful cyclization of the acylguanidine might result in heterocycles maintaining the crucial H-bond interactions to the catalytic aspartates, but with favourable pharmacokinetic properties as shown for BACE1.[34]

Supplementary data

Supplementary data associated with this article can be found, in the online version, at http://dx.doi.org/10.1016/j.bmcl.2014.07.054.

Reference and notes

1. Barrett, A. J. *Adv. Exp. Med. Biol.* **1977**, *95*, 291.
2. Davies, D. R. *Annu. Rev. Biophys. Biophys. Chem.* **1990**, *19*, 189.
3. Tang, J.; Wong, R. N. *J. Cell. Biochem.* **1987**, *33*, 53.
4. Hasilik, A.; Neufeld, E. F. *J. Biol. Chem.* **1980**, *255*, 4937.
5. Kornfeld, S. *Biochem. Soc. Trans.* **1990**, *18*, 367.
6. Conner, G. E.; Richo, G. *Biochemistry* **1992**, *31*, 1142.
7. Erickson, A. H.; Conner, G. E.; Blobel, G. *J. Biol. Chem.* **1981**, *256*, 11224.
8. Lee, A. Y.; Gulnik, S. V.; Erickson, J. W. *Nat. Struct. Biol.* **1998**, *5*, 866.
9. Richo, G. R.; Conner, G. E. *J. Biol. Chem.* **1994**, *269*, 14806.
10. Konttinen, Y. T.; Mandelin, J.; Li, T. F.; Salo, J.; Lassus, J.; Liljestrom, M.; Hukkanen, M.; Takagi, M.; Virtanen, I.; Santavirta, S. *Arthritis Rheum.* **2002**, *46*, 953.
11. Handley, C. J.; Mok, M. T.; Ilic, M. Z.; Adcocks, C.; Buttle, D. J.; Robinson, H. C. *Matrix Biol.* **2001**, *20*, 543.
12. Marciniszyn, J., Jr.; Hartsuck, J. A.; Tang, J. *J. Biol. Chem.* **1976**, *251*, 7088.
13. Umezawa, H.; Aoyagi, T.; Morishima, H.; Matsuzaki, M.; Hamada, M. *J. Antibiot. (Tokyo)* **1970**, *23*, 259.
14. Maynadier, M.; Vezenkov, L. L.; Amblard, M.; Martin, V.; Gandreuil, C.; Vaillant, O.; Gary-Bobo, M.; Basile, I.; Hernandez, J. F.; Garcia, M.; Martinez, J. *J. Controlled Release* **2013**, *171*, 251.
15. Lee, C. E.; Kick, E. K.; Ellman, J. A. *J. Am. Chem. Soc.* **1998**, *120*, 9735.
16. Whitesitt, C. A.; Simon, R. L.; Reel, J. K.; Sigmund, S. K.; Phillips, M. L.; Kevin Shadle, J.; Heinz, L. J.; Koppel, G. A.; Hunden, D. C.; Lifer, S. L.; Berry, D.; Ray, J.; Little, S. P.; Xiadong, L.; Marshall, W. S.; Panetta, J. A. *Bioorg. Med. Chem. Lett.* **1996**, *6*, 2157.
17. Dumas, J.; Brittelli, D.; Chen, J.; Dixon, B.; Hatoum-Mokdad, H.; König, G.; Sibley, R.; Witowsky, J.; Wong, S. *Bioorg. Med. Chem. Lett.* **1999**, *9*, 2531.
18. Cathepsin D activity was determined in a fluorescence-based assay that utilized the preferred CatD substrate sequence GKPILFFRLK(Dnp)-D-R-NH2 labeled with MCA (5 μM, Enzo Life Sciences, Lörrach). CatD isolated from human liver (1.4 nM, Sigma–Aldrich, Taufkirchen) cleaves the synthetic substrate to release fluorescence, which can then easily be quantified using a Perkin Elmer Envision multilabel reader at Ex/Em = 340/450 nm. As assay buffer 100 mM sodium acetate buffer pH 5.5, 0.25% CHAPS was used. The assay was performed in a kinetic mode. Pepstatin A was used as reference compound.
19. Renin enzymatic activity was determined in a fluorescence- based assay that utilized the quenched peptide substrate Dabcyl-g-Abu-IHPFHLVIHT-Edans (5 μM, Anaspec, Fremont CA). 10 nM human recombinant renin (Proteos, Kalamazoo, MI) was incubated with the substrate in 50 mM MOPS buffer, 0.1% Igepal, 0.5% BSA at 37 °C. The assay was run in a kinetic mode. The cleavage of the substrate was determined by release in fluorescence intensity with a Perkin Elmer Envision multilabel reader at Ex/Em = 340/495 nm. As reference compound renin inhibitor 2 (Sigma–Aldrich, Taufkirchen) was used.
20. Zaman, M. A.; Oparil, S.; Calhoun, D. A. *Nat. Rev. Drug Disc.* **2002**, *1*, 621.
21. Fobare, W. F.; Solvibile, W. R.; Robichaud, A. J.; Malamas, M. S.; Manas, E.; Turner, J.; Hu, Y.; Wagner, E.; Chopra, R.; Cowling, R.; Jin, G.; Bard, J. *Bioorg. Med. Chem. Lett.* **2007**, *17*, 5353.
22. Human recombinant Cathepsin D in complex with inhibitors was crystallized in 35% PEG2000, 0.1 M Na-Acetat (pH 5.5) in hanging drop by vapour diffusion at 20 °C. Crystals were cryoprotected in the mother liquor and X-ray diffraction data were collected at the PXIII beam line equipped with a Pilatus detector at the Paul Scherrer Institute in Villingen, Switzerland (see Supplemental Table 1). With the detector set at 250 mm, data were collected in 720 contiguous 0.25° oscillation images at 1 Å wavelength. Diffraction images were reduced, integrated and the intensities were merged and scaled using XDS.[35] The structures were solved by molecular replacement using Phaser version 2.3.0 in CCP4[36] with a previously published human CatD structure (PDB-ID: 1LYB)[37] as search model. After molecular replacement, manual rebuilding in Coot[38] followed by restrained refinements cycles using BUSTER version 2.11.1[39] yielded the final structures. In the final model building/refinement cycles, water molecules were inserted at stereo chemically reasonable sites that had features in electron density, and individual restrained B-values were refined. The quality of the final structures was assessed using ProCheck.[40]
23. The atomic coordinates and structure factors for the human CatD structures in complex with **2**, **7** and **24** have been deposited in the Protein Data Bank (www.rcsb.org) under the accession codes 4OC6, 4OBZ and 4OD9, respectively.
24. Klompmakers, A. A.; Hendriks, T. *Anal. Biochem.* **1986**, *153*, 80.
25. To activate Cathepsin D in the cartilage, the explants were incubated for 3 days at pH 5.5 at 37 °C and 7.5% CO_2. The pH in DMEM medium (+50 μg/ml ascorbic acid) was adjusted with MES (2-Morpholinethan–sulfonic acid Monohydrat). During the 3 days incubation time, the explants were treated with or without the potential CatD inhibitors. After 3 days the amount of sulphated GAGs as a major part of the cartilage were determined in the supernatant of explants. Increasing amount of GAG in the supernatant is a sign of cartilage destruction and should be reduced by the treatment of CatD inhibitors.
26. Majer, P.; Collins, J. R.; Gulnik, S. V.; Erickson, J. W. *Protein Sci.* **1997**, *6*, 1458.
27. SZMAP, version 2.1.0, OpenEye Scientific Software, Santa Fe, USA.
28. Feichtinger, K.; Sings, H. L.; Baker, T. J.; Matthews, K.; Goodman, M. *J. Org. Chem.* **1998**, *63*, 8432.
29. Kuhn, B.; Fuchs, J. E.; Reutlinger, M.; Stahl, M.; Taylor, N. R. *J. Chem. Inf. Model.* **2011**, *51*, 3180.
30. Barter, Z. E.; Bayliss, M. K.; Beaune, P. H.; Boobis, A. R.; Carlile, D. J.; Edwards, R. J.; Houston, J. B.; Lake, B. G.; Lipscomb, J. C.; Pelkonen, O. R.; Tucker, G. T.; Rostami-Hodjegan, A. *Curr. Drug Metab.* **2007**, *8*, 33.
31. Davies, B.; Morris, T. *Pharm. Res.* **1993**, *10*, 1093.
32. Iwatsubo, T.; Suzuki, H.; Sugiyama, Y. *J. Pharmacol. Exp. Ther.* **1997**, *283*, 462.
33. Clark, D. E. *Future Med. Chem.* **2011**, *3*, 469.
34. Oehlrich, D.; Prokopcova, H.; Gijsen, H. J. *Bioorg. Med. Chem. Lett.* **2014**, *24*, 2033.
35. Kabsch, W. *Acta Crystallogr., Sect. D* **2010**, *66*, 125.
36. McCoy, A. J.; Grosse-Kunstleve, R. W.; Adams, P. D.; Winn, M. D.; Storoni, L. C.; Read, R. J. *J. Appl. Crystallogr.* **2007**, *40*, 658.
37. Baldwin, E. T.; Bhat, T. N.; Gulnik, S.; Hosur, M. V.; Sowder, R. C.; Cachau, R. E.; Collins, J.; Silva, A. M.; Erickson, J. W. *Proc. Natl. Acad. Sci. U.S.A.* **1993**, *90*, 6796.
38. Emsley, P.; Cowtan, K. *Acta Crystallogr., Sect. D* **2004**, *60*, 2126.
39. Bricogne, G.; Blanc, E.; Brandl, M.; Flensburg, C.; Keller, P.; Paciorek, W.; Roversi, P.; Sharff, A.; Smart, O.S.; Vonrhein, C.; Womack, T.O., In: 2011.
40. Laskowski, R. A.; MacArthur, M. W.; Moss, D. S.; Thornton, J. M. *J. Appl. Crystallogr.* **1993**.
41. Molecular Operating Environment (MOE), 2. 1.; Chemical Computing Group, 1. S. St. W. S. #. M. Q. C. H. 2. 2.